Lithium Solvation and Mobility in Ionic Liquid Electrolytes with Asymmetric Sulfonyl-

Cyano Anion

Drace Penley<sup>1,‡</sup>, Xiaoyu Wang<sup>2,‡</sup>, Yun-Yang Lee<sup>1</sup>, Mounesha N. Garaga<sup>3</sup>, Raziyeh Ghahremani<sup>1</sup>,

Steve Greenbaum<sup>3</sup>, Edward J. Maginn<sup>2,\*</sup>, Burcu Gurkan<sup>1,\*</sup>

1. Chemical and Biomolecular Engineering, Case Western Reserve University, 10900 Euclid

Ave, Cleveland, OH, 44106

2. Chemical and Biomolecular Engineering, University of Notre Dame, Notre Dame, IN,

46556

3. Department of Physics and Astronomy, Hunter College, 695 Park Ave New York, New

York, 10065

<sup>‡</sup>Contributed equally

\* Corresponding: beg23@case.edu; ed@nd.edu

**Abstract** 

The solvation structure and transport properties of Li<sup>+</sup> in ionic liquid (IL) electrolytes based on n-

methyl-n-butylpyrrolidinium cyano(trifluoromethanesulfonyl)imide [PYR14][CTFSI] and

[Li][CTFSI]  $(0 \le x_{Li} \le 0.7)$  were studied by Raman and Nuclear Magnetic Resonance (NMR)

spectroscopy, and molecular dynamics (MD) simulations. At  $x_{Li} < 0.3$ ,  $Li^+$  coordination is

dominated by the cyano group. As x<sub>Li</sub> is increased, free cyano-sites becomes limited, resulting in

increased coordination via sulfonyl group. The 1:1 mixture of the symmetric anions

1

bis(trifluoromethanesulfonyl)imide ([TFSI]) and dicyanamide ([DCA]) results in similar physical properties to the IL with [CTFSI]. However, anion asymmetry is shown to increase Li-salt solubility and promote Li<sup>+</sup> transference. The lifetimes of Li<sup>+</sup>-cyano coordination for [CTFSI] are calculated to be shorter than for [DCA], indicating the competition from the sulfonyl group weakens its solvation with Li<sup>+</sup>. This resulted in higher Li<sup>+</sup> transference for the electrolyte with [CTFSI]. In relation to the utility of these electrolytes in energy storage, the Li-LiFePO<sub>4</sub> half cells assembled with IL electrolyte (x<sub>Li</sub>=0.3, 0.5, and 0.7) demonstrated a nominal capacity of 140 mAh/g at 0.1C rate and 90 °C where the cell with x<sub>Li</sub>=0.7 IL electrolyte demonstrated 61% capacity retention after 100 cycles and superior rate capability owing to increased electrochemical stability.

# Introduction

Ionic liquid (IL) electrolytes have shown to be a promising alternative to the state-of-the-art organic carbonate electrolytes for Li-metal and Li-ion batteries (LIBs) owing to their large electrochemical windows, negligible volatility, and non-flammability. 1-6 IL electrolytes are made entirely of discrete ions and have higher viscosities than organic carbonate electrolytes, which hinders Li+ transport in LIB applications. The addition of Li-salts to ILs results in strong interactions between Li<sup>+</sup> and the IL anion. There have been reports of ion aggregates in IL electrolytes with the increase of Li-salt concentration (0.01  $< x_{Li} < 0.4$ ).<sup>7, 8</sup> Such ion aggregates slow the vehicular motion of Li<sup>+</sup> where Li<sup>+</sup> moves with its solvation shell. However, the structural diffusion, where Li<sup>+</sup> jumps out of its solvation shell due to structural fluctuations or anion exchanges, is reported to gain significance towards higher Li-salt concentrations.<sup>9</sup> While the addition of excess Li-salt to IL electrolytes would intuitively lead to more cluster formation, several recent studies reported improved Li<sup>+</sup> transport, interfacial stability, and cycling with concentrated IL electrolytes in batteries. 10, 11 Similarly, enhanced Na+ transport was obtained in IL electrolyte with high Na-salt concentration (e.g.,  $x_{Na} = 0.5$ ) suitable for Na-ion batteries.<sup>12</sup> Therefore, understanding the metal ion coordination environment and transport as a function of Li-salt concentration in IL electrolytes and similarly concentrated electrolytes is important as it relates to battery performance.

Haskins et al.<sup>9</sup> studied the Li<sup>+</sup> solvation structure and transport in IL electrolytes with Li-salt (0.05  $\leq$ x<sub>Li</sub>  $\leq$  0.33). They reported that the anion size, Li<sup>+</sup>-anion binding strength, and liquid density are the key factors in determining Li<sup>+</sup> transport. With [TFSI] based electrolyte, the higher liquid density, the stronger Li<sup>+</sup>-[TFSI] interaction, and the longer ion-pair lifetime leads to slower Li<sup>+</sup>

transport, compared to the smaller tetrafluoroborate ([BF<sub>4</sub>]) and bis(fluorosulfonyl)imide ([FSI]). Although the contribution to  $Li^+$  diffusivity due to anion exchange is less than 40%, it is found to gain significance at higher Li-salt concentration ( $x_{Li}$ =0.33); especially with larger anion size the contribution to  $Li^+$  diffusivity due to anion exchange increases.

In an attempt to overcome the strong interactions between the IL anion and the Li<sup>+</sup> cation, and improve the battery performance in terms of rate capability, IL electrolytes with mixed anions have been studied. 13-18 Bayley et al. 18 showed that at a fixed Li<sup>+</sup> concentration, substituting some of the [TFSI] anion with [FSI] in an IL electrolyte with an n-methyl-n-propylpyrrolidinium ([PYR13]) cation results in an increased Li<sup>+</sup> diffusivity. They found that increasing the ratio of [FSI] anion in the mixtures from 20% to 80% leads to an enhanced Li $^+$  diffusion coefficient (from 5 imes 10 $^{-12}$  to 1 × 10<sup>-11</sup> m<sup>2</sup>s<sup>-1</sup> at room temperature). Huang et al. <sup>16</sup> reported on the IL mixture of 1-ethyl-3methylimidazolium dicyanamide ([EMIM][DCA]) and [PYR13][TFSI] where a preferential coordination of Li<sup>+</sup> by [DCA] over [TFSI] was shown by a combined Raman spectroscopy and molecular dynamics (MD) simulations study. Further conductivity loss with the increase of Li-salt concentration (from 0.5 to 1M) was prevented despite the continued increase in viscosity. This was because the Li<sup>+</sup> coordination number (CN) of 3 to 4 was maintained throughout the changes in Li-salt composition (0.01  $\leq$  x<sub>Li</sub>  $\leq$  0.15 or 1M) whereas the concentration-dependent Li<sup>+</sup>-[TFSI] coordination was diminished. Furthermore, the addition of [DCA] allowed for shorter ion-pair lifetimes for Li<sup>+</sup>, as calculated by MD. In another study by Lesch et al., <sup>19</sup> [EMIM] cation was compared with [PYR13] in terms of the transport properties in the IL electrolytes with [TFSI] anion. They found that [PYR13] cation allowed for faster exchange of [TFSI] within the first solvation shell of Li<sup>+</sup>, despite the overall slower dynamics. Specifically, the interaction between

the [PYR13] cation and [TFSI] prevented the bridging of two or more Li<sup>+</sup> by the anion. These studies demonstrated the influence of both anions and cations in IL electrolytes towards enhancing the Li<sup>+</sup> transport.

Concentrated electrolytes including ILs with asymmetric anions have also been studied in terms of their influence on Li<sup>+</sup> transport.<sup>20-22</sup> When referring to asymmetry in anions in the context of Li<sup>+</sup> solvation, coordination via two or more functional cites of differing chemistries is possible. For example, cyano(trifluoromethansulfonyl)imide ([CTFSI]) shown in **Table 1**, contains the coordination chemistries (S=O and C≡N) of both of the symmetric parent anions [TFSI] and [DCA]. With the asymmetric anions, Li-salt concentrations above  $x_{Li} > 0.4$  were also possible<sup>23</sup> in contrast to the IL electrolytes with the symmetric [TFSI] and [FSI] where crystallization occurs at room temperature.<sup>24, 25</sup> Brinkkötter et al. studied the migration of Li<sup>+</sup> in a pyrrolidinium based IL electrolyte with (fluorosulfonyl)(trifluoromethanesulfonyl)imide ([FTFSI]) anion using electrophoretic NMR.<sup>20</sup> They found that vehicular mechanism dominated the Li<sup>+</sup> transport up to the concentration range of x<sub>Li</sub>=0.4. The net negative charge of the Li-solvate cluster due to multiple anions coordinating Li<sup>+</sup> resulted in the migration of Li<sup>+</sup> towards the positive electrode. However, they noted that as the Li<sup>+</sup> concentration increased, the exchange of the Li<sup>+</sup> between clusters also increased. They also found that Li<sup>+</sup> motion was less correlated with [FTFSI] anions in comparison to [TFSI] containing IL electrolytes. Therefore, it remains of interest to examine the Li<sup>+</sup> solvation and transport in concentrated IL electrolytes with asymmetric anions.

It is also of interest to establish the relevance of IL electrolytes with asymmetric anions for LIBs. Hoffknecht et al.<sup>26</sup> studied the cyclic performance of LIB NMC (Nickel Manganese Cobalt Oxide)

cathode with IL electrolyte based on n-methyl-n-butylpyrrolidinium cation ([PYR14]) and the asymmetric [CTFSI] anion. The IL did not crystallize at low temperatures ( $T < -100^{\circ}$ C), possessing a glass transition temperature of -97.8°C. It also showed higher ionic conductivity than [TFSI] and [FTFSI] systems. The [CTFSI] based electrolyte containing 0.4 M of [Li][CTFSI] (estimated x<sub>Li</sub>~0.08) demonstrated higher thermal and anodic stability (4.5 V vs Li/Li<sup>+</sup>) compared to the ILs with [DCA], [TFSI], and [FTFSI] anions. It is not clear how the asymmetric anion influenced the transport mechanism in the LIBs tested where improved battery cycling performance was reported compared to the symmetric anions. Since they included electrolyte additive to suppress interfacial side reactions, it is difficult to decouple the bulk transport from the interfacial effects. Recently, Nurnberg et al. 22 studied Li<sup>+</sup> solvation in [PYR14][CTFSI] electrolyte by Raman and Nuclear Magnetic Resonance (NMR) spectroscopic studies. They found that the cyano-group of [CTFSI] dominated the coordination environment up until a Li-salt fraction of 0.4 and beyond this concentration, the coordination through the S=O sulfonyl group became apparent. While [CTFSI] based electrolytes showed lower conductivity compared to [TFSI], they observed a shift from vehicular to hopping transport mechanisms with [CTFSI] at higher concentrations of  $Li^+$  (x = 0.6 to 0.7), supported by the NMR results. However, it remains unclear how the anion asymmetry in IL electrolyte alters the Li-solvate structures and Li<sup>+</sup> transference, differently than diffusion, in a way that improves cycling performance in LIBs.

The percentage of charge carried by Li<sup>+</sup> ions in the electrolyte is represented as the transference number. Transference number is commonly estimated by the Bruce-Vincent electrochemical polarization method<sup>27</sup> and Pulse-Field-Gradient NMR (PFG-NMR) spectroscopy.<sup>28</sup> These two techniques have been used readily in previous studies to compute the Li<sup>+</sup> transference in various

battery electrolyte systems. 6, 15, 29-34 However, it should be noted that PFG-NMR does not account for hindrances in Li<sup>+</sup> transport due to anion-blocking conditions, where applied potential and solvation by IL anions impede the diffusion of Li<sup>+</sup>, as reported by Brinkkötter et al.<sup>20</sup> Huang et al. 15 studied the Li<sup>+</sup> transference in a mixture of [PYR13][TFSI] and [PYR13][FSI] (1:1, v/v) with 0.5M [Li][FSI] by the polarization method. This ternary IL electrolyte with [FSI] and [TFSI] mixture provided a slightly higher transference number (0.18) compared to the binary [FSI] (0.15) and [TFSI] (0.17) IL electrolyte systems. To account for the varying Li<sup>+</sup> mole fractions, the transference numbers were normalized by Li<sup>+</sup> mole fraction and the resulting transference with [TFSI]:[FSI] ternary IL was the same to that of the binary mixture, thus indicating that the addition of the [FSI] anion to [TFSI] helps improve the charge carrier ability of Li<sup>+</sup>. They also observed the depression of the freezing point in the mixed IL compared to the parent compounds which enabled the operation of lithium iron phosphate (LFP) half cells with liquidus electrolyte at sub-zero temperatures (-20 °C). 15 Sälzer et al. 29 also studied the Li<sup>+</sup> transference number in [Li][FSI]:[PYR13][FSI] (40:60) and [Li][FSI]:tetraglyme (50:50) electrolytes. They employed the polarization method in Li|Li symmetric cells and compared the transference number results against those obtained by PFG-NMR method. The transference numbers determined by the polarization method for the [Li][FSI]:tetraglyme were roughly 30 times lower than those calculated by PFG-NMR. On the other hand, the calculated values for [Li][FSI]:[PYR13][FSI] were only slightly lower. We interpret from these results that in IL electrolytes where IL cation can exchange momentum with both Li<sup>+</sup> and the IL anion, the impact of anion blocking on Li<sup>+</sup> transference is less pronounced, and the PFG-NMR provides a good estimate for transference numbers. The electrophoretic NMR would be ideal to study transference in LIBs; however, it is a sophisticated instrument that is not commonly available.

These previous studies elucidate the importance of understanding the solvation of Li<sup>+</sup> in IL-based systems in creating effective and safe electrolytes for future LIBs. However, it remains unclear how the anion asymmetry in IL electrolytes influence solvation properties and macroscopic and microscopic transport properties in comparison to the simple mixtures of symmetric anions with different Li<sup>+</sup> coordination chemistry. In this work, we combine physical properties measurements, Raman spectroscopy, and NMR with MD simulations to gain insight into the solvation structure and dynamics of [PYR14][CTFSI]:[Li][CTFSI] comparison in to [PYR14][DCA]:[PYR14][TFSI]:[Li][TFSI] electrolytes. We also studied the electrochemical stability of these electrolytes with and without Li-salt. [PYR14][CTFSI] with  $x_{Li} = 0.3, 0.5, and$ 0.7 were employed in Li|LFP coin cells and their rate capabilities were tested at 25 and 90 °C and varying C-rates. The measured impact of asymmetry and the different coordination sites of the anion on the Li<sup>+</sup> solvation and diffusion demonstrate the possibility of enhancing Li<sup>+</sup> transport and electrochemical stability in concentrated IL electrolytes. This observation is supported by the rate capability and cyclability tests.

# **Experimental Methods**

#### **Materials**

**Table 1** reports the name, abbreviation, supplier, mole fraction purity, water mass fraction, and chemical structure and the physical state of all the ILs and Li-salts that were used in this study.

**Table 1.** Name, abbreviation, supplier, purity (as supplied), water content, and chemical structure of the ILs (liquids at room temperature) and Li-salts (solids at room temperature) used in this study.

Name	Abbreviation	Supplier	Mole Fraction Purity	Water Content (mass fraction)
N-methyl-n-butylpyrrolidinium cyano(trifluoromethanesulfonyl)i mide	[PYR14][CTF SI]	Provisco	0.98	0.000041
N C N CF3	T.			
N-methyl-n-butylpyrrolidinium bis(trifluoromethanesulfonyl)imi de	[PYR14][TFSI ]	Iolitec	0.99	0.000074
$CF_3$ $N$ $N$ $N$ $N$	F <sub>3</sub>			
N-methyl-n-butylpyrrolidinium dicyanamide	[PYR14][DCA ]	Iolitec	0.98	0.000088
N = C = N	 			
Lithium bis(trifluoromethanesulfonyl)imi de	[Li][TFSI]	TCI Chemicals	0.98	-
Lithium cyano(trifluoromethanesulfonyl)i mide	[Li][CTFSI]	Provisco	0.98	-

Cannon oil viscosity standards (N100 and S20) were purchased from RheoSense (San Ramon, CA). The [PYR14][DCA]:[PYR14][TFSI] sample was prepared with a 1:1 molar ratio. The Lisalt was dissolved in the IL or binary IL mixtures in mole fractions of  $x_{Li} = 0.05$ -0.70. LiFePO<sub>4</sub>

(LFP) powder, conductive graphite powder (CG; >99.98%), Al-clad CR2032 case, and precoated LFP electrode sheet with an active material coating density of 12 mg cm<sup>-2</sup> were purchased from MTI (Richmond, CA). Poly(vinylidene fluoride) (PVdF, M<sub>w</sub>: 534 kDa) was purchased from Millipore Sigma (Burlington, MA). Glass fiber nonwoven separator (Whatman grade GF/A, 260 μm in thickness) was purchased from VWR (Radnor, PA). All mixtures were prepared and stored in a glovebox (VTI Super Glove Boxes) with < 1 ppm of water and oxygen under an argon atmosphere. The exact compositions of the systems studied both experimentally and computationally are listed in **Table S1** in terms of Li-salt mole fraction, molality, and the number of species in the simulation box.

# **Density**

Densities of all IL mixtures were measured in the temperature range of 298–323 K by an Anton Paar DMA 4500M vibrating tube densitometer ( $\pm 0.03$  K,  $u(\rho) = 0.00005$  g/cm<sup>3</sup>) with a sample size of 1 mL. Prior to testing each IL, the densities of air and water were measured at 25 °C to confirm the accuracy of the instrument. The vibrating tube was rinsed between ILs with methanol followed by deionized water, and the density of air and water were checked again. The water content of ILs was measured before density measurements by Coulometric Karl Fischer Titration (Metrohm Coulometric KF 889D).

#### Viscosity

Viscosity was measured with a RheoSense MicroVISC microchannel viscometer inside a RheoSense MicroVISC Temperature Control unit (±0.10 K). The sample flowed through the microchannel at a flow rate of approximately 0.75 μL s<sup>-1</sup>. A single measurement required

approximately 10-20  $\mu$ L of sample. Before testing each IL, the microchannel chip was rinsed with methanol followed by rinsing with deionized water. The uncertainty in measured viscosities was determined from the measurements of Cannon oil viscosity standards. Accordingly, the estimated standard uncertainty is  $u(\mu) = 0.02$ .

To express the temperature dependence of the measured viscosities, Vogel-Fulcher-Tammann (VFT)<sup>35, 36</sup> equation (eqn. 1) was used to fit the data:

$$\mu = \mu_0 \times e^{\frac{A}{T - T_0}} \tag{1}$$

where A (mPa s) represents the viscosity at and infinitely high temperature, and B (K) and  $T_0$  (K) are fitting parameters, with  $T_0$  representing an ideal glass transition temperature ( $T_g$ ), usually  $\sim$  50K below the experimentally observed  $T_g$ .

# **Conductivity**

Conductivity of the liquid samples was measured with a dual platinum electrode cell (MMA 500, Materials Mates Italia) with a cell constant of 1.41 cm<sup>-1</sup> by electrochemical impedance spectroscopy using BioLogic SP-240 potentiostat equipped with frequency response analyzer (7 MHz–10  $\mu$ Hz). The temperature was controlled for conductivity measurements by placing the cell inside the RheoSense MicroVISC Temperature Control unit (±0.10 K). The solution resistance was determined from the intercept of a linear fit to the capacitive region of the Nyquist plot (imaginary versus real impedance). The estimated standard uncertainty is  $u(\sigma) = 0.05$ .

Similar to temperature-dependent viscosities, VFT equation (eqn. 2) was used to fit the conductivity data:

$$\sigma = \sigma_0 \times e^{\frac{-B}{T - T_0}} \tag{2}$$

where  $\sigma_0$  (mS/cm) represents the conductivity at and infinitely high temperature and C (K) is a fit parameter.

# **Solvation by Raman Spectroscopy**

Raman spectra were collected using a Horiba Xplora One Raman system with a 785 nm excitation laser and a spectral range of 700-2250 cm<sup>-1</sup>. The S-N-S stretching of [TFSI] and S-N-C stretching of [CTFSI] are expected to be in the 700-800 cm<sup>-1</sup> and 1075-1175 cm<sup>-1</sup> regions, respectively. The C $\equiv$ N stretch of both [DCA] and [CTFSI] is expected in the 2150-2250 cm<sup>-1</sup> region. The spectra were collected using a 20× magnification objective, 1000  $\mu$ m hole, 200  $\mu$ m slit, 10 s exposure time, and 10 accumulations. The spectral resolutions were 1.12 cm<sup>-1</sup> for the 700-800 cm<sup>-1</sup> region, 1.03 cm<sup>-1</sup> for the 1075-1175 cm<sup>-1</sup> region, and 0.79 cm<sup>-1</sup> for the 2150-2250 cm<sup>-1</sup> region. The base line correction was performed by using the standard normal variate method, which entails subtracting the mean intensity of the spectra and dividing by the standard deviation. Then, the spectra were normalized according to the largest intensity peak. The peak deconvolution was done using the Igor Pro 8.04 software. The goodness of the multi-peak fits were found as  $\chi^2 < 0.1$ .

Coordination number (CN) analysis is done to understand the Li<sup>+</sup> solvation environment using a modified method that was first introduced by Lassegues et al.<sup>37</sup>, shown in (eqn. 3).

$$\frac{A_{II} + A_{III}}{(A_I + A_{II} + A_{III})} = n \cdot x_{Li} \tag{3}$$

where  $A_I$  represents the peak area of free sites of the anion,  $A_{II}$  and  $A_{III}$  represents the area of coordinated sights of ion-pairs (Li<sup>+</sup>-[CTFSI]) and clusters (Li<sup>+</sup>-[CTFSI]-Li<sup>+</sup>), respectively,  $x_{Li}$  is Li<sup>+</sup> mole fraction, and n is CN. Accordingly, the CN represent the number of coordinated sites and not necessarily the coordinated number of anions. [TFSI] has a total of four sites where Li<sup>+</sup> can

coordinate to the oxygens (Li-O), [DCA] has two sites where  $Li^+$  can coordinate with the terminal nitrogens in the cyano groups (Li-CN), and [CTFSI] has three sites: 2 Li-O(=S) and 1 Li-N(=C).

# Diffusivity and Transference Measurements by NMR

Diffusion coefficients of ions in ILs electrolytes were measured on a Varian-Agilent 300 MHz NMR spectrometer operating at a magnetic field of 7T ( $^{1}$ H,  $^{19}$ F, and  $^{7}$ Li Larmor frequencies of 300, 284.4 and 116.6 MHz, respectively) equipped with DOTY Z-spec PEG-NMR probe. The signal was accumulated over 16 - 32 transients with 2 - 3 s recycling delay. The diffusion coefficients were measured at 26, 55, and 90 °C by using a spinecho pulse sequence. The gradient strength was varied in the range of 10 - 800 G/cm for 16 increments. The diffusion time ( $\Delta$ ) and the diffusion pulse length ( $\delta$ ) were set to 50 - 200 ms and 2 - 3.5 ms, respectively. The diffusion coefficients were calculated using the well-known Stejskal-Tanner equation.  $^{28}$ 

The transference number of  $\text{Li}^+(t_{NMR}^+)$  was estimated using the measured diffusivities following equation 4:

$$t_{NMR}^{+} = \frac{x_{Li} + D_{Li} + x_{anion(s)} D_{anion(s)} + x_{[PYR14]} D_{[PYR14]}}{x_{Li} + D_{Li} + x_{anion(s)} D_{anion(s)} + x_{[PYR14]} D_{[PYR14]}}$$
(4)

Where x and D represent the mole fraction and diffusion coefficient, respectively for Li<sup>+</sup>, [PYR14], and the anions as indicated in the subscripts. In the case of the mixed-anion system,  $x_{anion(s)}$  and  $D_{anion(s)}$  represent sum of [DCA] and [TFSI].

## **Electrochemical Stability**

Linear sweep voltammetry (LSV) of the ILs was conducted to evaluate the electrochemical stability windows. A three-electrode cell configuration was used consisting of a glassy carbon (GC) working electrode (BASi, 3 mm dia.), a coiled platinum (Pt) wire counter electrode (1 mm dia.), and a Pt wire quasi-reference electrode (1 mm dia.). The anodic and cathodic sweeps were collected separately starting from zero potential on a freshly polished GC electrode. The voltage scan rate was 20 mVs<sup>-1</sup>. The sample volume was roughly 0.5 mL. The LSVs were performed in a positive-pressure nitrogen glovebox (Terra Universal).

# Li-LFP Cell Assembly and Tests

A slurry of LFP:CG:PVdF (80:10:10) was cast onto an aluminum current collector with a wet film thickness of 15 μm. The electrode was immediately transferred into an 80 °C oven for 1h, and then transferred to a vacuum oven at 100 °C to remove any residual moisture overnight. An electrode with a diameter of 5/8 in. was cut via a puncher and weighed by a balance (Sartorius QUINTIX65-1S). The average coating density of the resulting LFP electrode was about 3 mg cm<sup>-2</sup>, which is the number used in the charge/discharge rate performance calculations. Under an argon atmosphere, the IL electrolytes with x<sub>Li</sub>=0.3, 0.5, and 0.7 (homogenous liquid or gel) were preheated to 80 °C and about 100 μl of each sample was used to wet the glass fiber separator that was placed on a LFP electrode in an Al-clad CR2032 casing. The wetted separator, electrode and casing assembly was transferred into a sealed container with vacuum capability and kept under 80 °C overnight to allow for complete wetting of the porous separator and electrode. The container was then disconnected from vacuum and brough into the glovebox to ensure the contents are not exposed to air. The final assembly of the cell was sealed by an automatic crimper (MTI) inside the glovebox.

The fabricated cells were cycled between 2.5 and 3.8 V at 0.1, 0.2, 0.5, and 1 C with constant current (CC) at 25 and 90 °C. Electrochemical impedance spectroscopy (EIS) was performed before and after the cycling at open circuit voltage (OCV) between  $10^{-2}$  and  $10^{5}$  Hz with a voltage amplitude of 10 mV. Temperature control was done via Espec BTZ-133 temperature chamber ( $\pm 0.5$ K). CVs of the Li-LFP batteries were performed at a scan rate of 0.05 mV s<sup>-1</sup> at 90 °C following the rate performance test. The Li<sup>+</sup> diffusion within the LFP electrode was measured by the Galvanostatic Intermittent Titration Technique (GITT), where a CC pulse sequence of 0.1 C was carried out for 1h, followed up by a relaxation time of 2h. Li<sup>+</sup> diffusion into LFP was calculated by equation (5), where L is the diffusion length (which is the thickness of LFP electrode measured to be  $6 \pm 0.1 \,\mu\text{m}$ ),  $\tau$  is the relaxation time after pulse sequence (2 h),  $\Delta E_s$  is the steady-state potential difference after a single CC pulse sequence (Es-E1), and  $\Delta E_t$  is transient overpotential (E3-E2).

$$D_{Li^+,LFP} = \frac{4L^2}{\pi\tau} (\frac{\Delta E_s}{\Delta E_t})^2 \tag{5}$$

# **Computational Methods**

# **Molecular Dynamics (MD) Simulations**

The General Amber Force Field <sup>38</sup> (GAFF) was used to describe both the inter- and intra- molecular interactions. Geometries of all cations and anions were first optimized using density functional theory at the B3LYP method with the cc-PVTZ basis set <sup>39</sup>. Single point energy calculations based on the optimized structure were used to provide a three-dimensional electrostatic grid map from which RESP <sup>40</sup> charges were calculated using Antechamber. <sup>41</sup> In this work, we use ab initio calculations to estimate the partial charges. A neutral ion pair [PYR14][CTFSI] was optimized

using DFT-B3LYP, followed by a RESP point charge calculation scheme. We found partial charges were around 0.7 for the different anions, and so we set a common value of 0.7 as the scaling factor for all of the systems for charge transfer and polarization.<sup>42</sup> Lennard-Jones, bond, angle, dihedral and improper parameters are taken directly from the GAFF library.

The LAMMPS<sup>43</sup> software package was used as the MD engine and the analysis of the generated trajectories was performed with the Travis package.44,45 The simulations employed a Lennard-Jones cut off distance of 12 Å with tail corrections applied to compensate for the long-range van der Waals interactions contribution to the energy and pressure. The Lorentz-Berthelot combining rule was used to calculate cross interactions. Long range electrostatic interactions were modeled using a particle-particle particle-mesh solver, 46 which provides comparable accuracy with faster speed than the traditional Ewald method. Nosé-Hoover style non-Hamiltonian equations of motion were used for both the thermostat (with a time constant of 100 fs) and the barostat (with a time constant of 1000 fs). A time-step of 1 femtosecond was used for all the simulations. 400 cations and 400 anions were initially packed into a cubic simulation box with a length of 55 Å on each dimension using PACKMOL<sup>47</sup>. Each simulation underwent an isothermal-isobaric (NPT) relaxation with a length of 2 nanoseconds to allow fully equilibration, from which density was sampled. The computed average density was then used to perform canonical ensemble (NVT) simulations for another 20 nanoseconds, from which the structural and dynamic information were sampled. Example LAMMPS input files and data files containing all simulation details are provided in the Supporting Information.

## **Computational Analysis**

The radial distribution function (RDF), spatial distribution function (SDF) and the mean squared displacement (MSD) calculations were performed using the Travis code.<sup>44</sup> The simulated CN is defined by the number of coordinating sites within the first solvation shell defined by the distance of the first local minimum in the RDF (R<sub>c</sub>). R<sub>c</sub> values of 0.325 nm and 0.452 nm were used for calculating CN for Li-N(≡C) and Li-O(=S), respectively. The shear viscosity was calculated using a time decomposition bootstrap method.<sup>48</sup> The ionic conductivities were calculated using the Nernst-Einstein equation.<sup>49</sup>

To calculate the ion-pair lifetimes for a specific cation-anion pair, we first calculated the pairwise site-to-site radial distribution functions. The site for Li-N( $\equiv$ C) coordination was the terminal nitrogen and the site for Li-O( $\equiv$ S) was calculated by using the center-of-mass of the entire sulfonyl group. Setting the center-of-mass of the entire sulfonyl group as the site rather than using an individual oxygen was done to avoid double counting Li<sup>+</sup> that are coordinating with both oxygens. A delta function (eqn. 6) was used to describe whether a particular cation of species i and a particular anion of species j are forming an ion pair.

$$\delta_{ij}(t) = \begin{cases} 1 & \left( R_{ij} \le R_c \right) \\ 0 & \left( R_{ij} > R_c \right) \end{cases} \tag{6}$$

From this, an overall ion pair correlation function  $c(\tau)$  was computed as

$$c(\tau) = \frac{1}{N_i N_j} \sum_{i=1}^{N_i} \sum_{j=1}^{N_j} \int_0^\infty \delta_{ij}(t) \cdot \delta_{ij}(t+\tau) dt$$
 (7)

where the summations are over the number of cations  $(N_i)$  and anions  $(N_j)$ . To eliminate numerical noise, each correlation function was fit to a triple exponential and the integral in eqn 7 was performed analytically.

#### **Results**

# **Physical Properties of IL Electrolytes**

Experimental and computed densities as well as viscosities of all ILs without Li-salt are shown in Figures S1 and S2, respectively. The computed densities are all within 2% of the experimental densities. The computed viscosities consistently overestimate the experimental viscosities by about 40%, but capture the relative viscosity trend across different ILs. The 1:1 mixture of [PYR14][TFSI] and [PYR14][DCA] has a density and viscosity that are roughly the average of the two pure ILs, indicating that the mixture is ideal. Moreover, the 1:1 mixture has a similar density and viscosity as [PYR14][CTFSI]. The temperature-dependent densities, viscosities, and conductivities for [PYR14][CTFSI] (Table S2) in our measurements agree with the previous report by Hoffknecht et al.<sup>26</sup> In comparison to the binary IL mixture with [TFSI]:[DCA] (1:1) (purple diamonds in Figure 1a), the density of the [PYR14][CTFSI] (black squares in Figure 1a) is slightly lower which suggests the ions do not pack as tightly as in the binary mixture. However, for these same systems the measured viscosities and conductivities are the same as seen in **Figure** 1b and c, respectively. The computations slightly overestimate the densities, viscosities and conductivities (hollow symbols in Figure 1), however captured the same dependence on temperature and Li-salt concentration. The largest deviation comes from the x<sub>Li</sub>=0.2 [CTFSI] system, we think this is resulted from the charge scaling scheme we developed for pure IL systems - at higher Li concentration, the potential model fails to predict the properties. However,

combining the underestimation of the viscosity for  $x_{Li}$ =0.2 [CTFSI] in **Figure 1b**, we should expect such overestimation of conductivity. Besides the inaccuracy of the potential model, the ionic conductivity of the ionic liquid systems is challenging to compute, since it relies on substantial amount of data to ensure sufficient averaging.<sup>50</sup>

The addition of Li-salt resulted in increased densities and viscosities, and decreased conductivities as seen in **Figure 1a**, **b**, and **c**, respectively. The only exception to this observation was the computed densities of [Li][DCA] in [PYR14][DCA] where an initial sharp decrease in density was observed at x<sub>Li</sub>=0.05, shown in **Figure S3a**. This is potentially a result of increased structural ordering at low Li-salt concentrations. For all other systems where density increases, the free volume that results from loose packing of the IL cations and anions gets occupied by Li<sup>+</sup>. This allows Li<sup>+</sup> to interact with the associating site on the anion, thus resulting in the decrease of free volumes and increase of densities.<sup>51-53</sup>

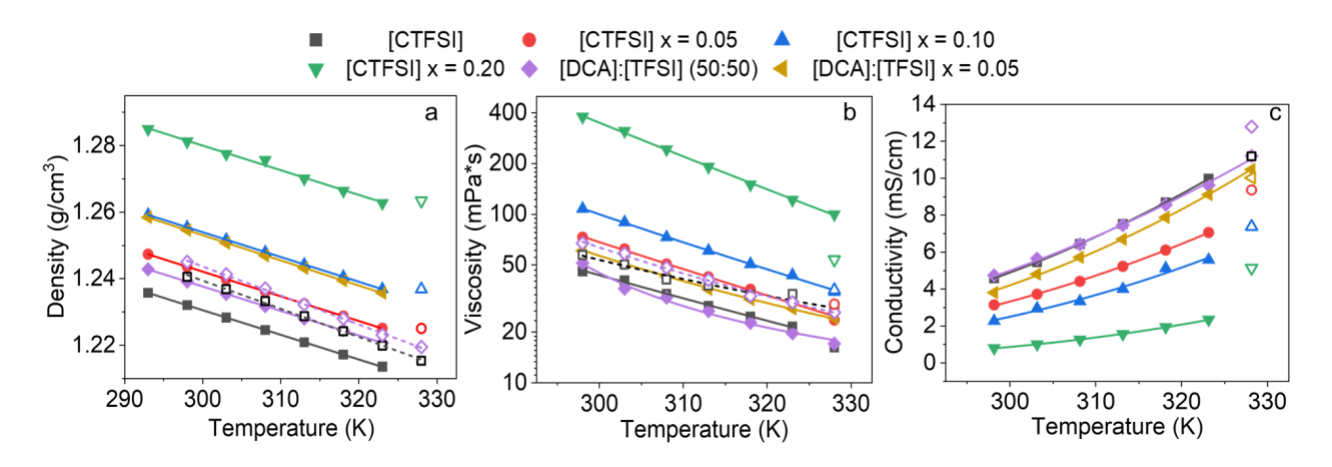


**Figure 1.** Experimental (filled symbols) and computed (hollow symbols) densities (**a**), viscosities (**b**), and conductivities (**c**) of IL electrolytes as a function of temperature and Li-salt concentration ( $x_{Li}$ =0.05, 0.1, and 0.2). Note that higher Li-salt concentrations yielded a gel ( $x_{Li}$  = 0.5 and 0.7)

and did not have flow characteristics to measure viscosity or density within the capabilities of the described methods and instruments. Densities were fit with linear trend lines; viscosities and conductivities were fit to VFT to express the temperature dependence (see **Table S3** and **S4** for fit parameters).

Interestingly, the [DCA]:[TFSI] mixture at x<sub>Li</sub>=0.05 had lower viscosity and higher conductivity than the [CTFSI] electrolyte at the same Li-salt concentration despite its higher density. This is possibly due to the preferential solvation of Li<sup>+</sup> by [DCA] over [TFSI] in the binary IL, which we have previously observed in a similar mixture<sup>16</sup>, that leads to a more compact liquid. Despite the compactness, the solvated Li<sup>+</sup> by the smaller [DCA] anion is more mobile compared to the Li-solvate by the larger [CTFSI] anion. We were unable to measure the properties of the [DCA]:[TFSI] mixture electrolyte with Li-salt concentrations higher than x<sub>Li</sub>=0.05 since those samples were not homogenous liquids. It should be noted that even for the x<sub>Li</sub>=0.05 solution for the [DCA]:[TFSI] system the solution was cloudy, which is indicative of phase separation at the microscopic level. Conversely, we were able to produce completely homogenous mixtures with [CTFSI] electrolytes up to x<sub>Li</sub>=0.7 (see **Figure S4** for the photos of samples showing the state of the mixtures). This is consistent with previously reported solutions containing asymmetric anions capable of producing high Li-salt concentration electrolytes.<sup>21, 23</sup>

# Li<sup>+</sup> Solvation Structure

Raman spectroscopy was used to analyze the CN with increasing Li-salt concentration. It also provided direct comparison with the CN from MD simulations. The local spectra of

[PYR14][CTFSI] with  $x_{Li}$ =0.05, 0.1, 0.2, 0.5, and 0.7 in the regions of 700-800, 1075-1175, and 2150-2250 cm<sup>-1</sup> are shown in **Figure 2a-c**.

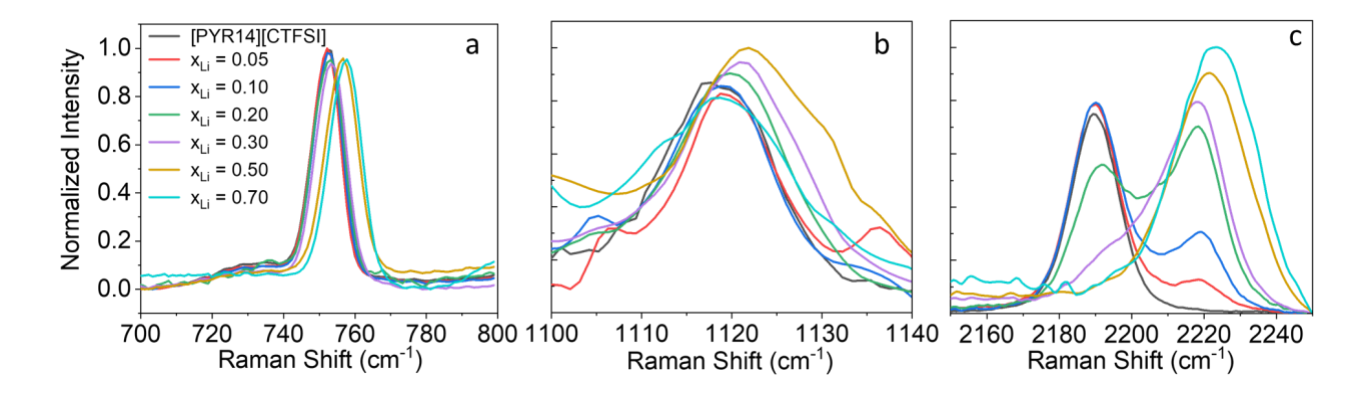


**Figure 2.** Raman spectra of [PYR14][CTFSI] with  $x_{Li}$ =0.05, 0.1, 0.2, 0.3, 0.5, and 0.7: (a) spectral region of 700-800 cm<sup>-1</sup> for the S-N-C symmetric stretch; (b) 1110-1140 cm<sup>-1</sup> for the S=O symmetric stretch; (c) 2150-2250 cm<sup>-1</sup> for the C $\equiv$ N symmetric stretch. With the addition of [Li][CTFSI] at 0.5 and 0.7, the S-N-C is blue-shifted corresponding to the Li<sup>+</sup> coordination. For the S=O and C $\equiv$ N stretch regions, peak deconvolution was performed (examples in **Figures S5-S6**). At  $x_{Li}$ =0.5 and 0.7, all of the N( $\equiv$ C) sites appear to be coordinated to Li<sup>+</sup> with a single vibration peak.

As seen in **Figure 2a**, there is minimal shift in the S-N-C (755 cm<sup>-1</sup>) peak until  $x_{Li}$ =0.5, due to sulfonyl coordination. This is due to the domination of the cyano coordination  $Li^+$ -N( $\equiv$ C) at these concentrations, which is seen in the 2150-2250 cm<sup>-1</sup> region (**Figure 2c**) where spectral changes are clear. With increasing Li-salt concentration, the C $\equiv$ N symmetric stretch at 2190 cm<sup>-1</sup> decreases and the peak at 2220 cm<sup>-1</sup> increases. At both  $x_{Li}$ =0.5 and 0.7, the 2190 cm<sup>-1</sup> peak is absent, suggesting that all of the N( $\equiv$ C) sites are coordinated with Li<sup>+</sup>. Li<sup>+</sup>-O( $\equiv$ S) coordination becomes

apparent as x<sub>Li</sub> increases, which causes a shift in the S-N-C peak to about 758 cm<sup>-1</sup> (x<sub>Li</sub>=0.5 and 0.7) (**Figure 2a**) and S=O peak to about 1130 cm<sup>-1</sup> ( $x_{Li}$ =0.3, 0.5, and 0.7) (**Figure 2b**). This can be seen as well in the CN analysis shown in Figure 3, where Li-O(=S) coordination does not appear until x<sub>Li</sub>=0.3, consistent with previously reported CNs for [CTFSI].<sup>22</sup> The areas of the peaks corresponding to the coordinated and free anion sites were determined from the deconvoluted spectra at the 1110-1140 cm<sup>-1</sup> (Figures S5) and 2150-2250 cm<sup>-1</sup> (Figures S6) regions for S=O and C $\equiv$ N modes, respectively. It should be noted that the spectra for Li-N( $\equiv$ C) was deconvoluted into 3 peaks for  $0.05 < x_{Li} \le 0.3$  as the second derivative analysis suggested the existence of three peaks in this region. These three peaks correspond to N(≡C) vibrations of the anion that is not coordinated with Li<sup>+</sup> at 2190 cm<sup>-1</sup>, coordinated N( $\equiv$ C) with a single Li<sup>+</sup> (ion-pair) around 2220 cm<sup>-1</sup>, and coordination with multiple Li<sup>+</sup> due to the additional O(=S) site on the same anion (aggregate) around 2205 cm<sup>-1</sup>. We see small peak shifts (< 3 cm<sup>-1</sup>) in Figure 2b due to O(=S) coordination at  $x_{Li} < 0.30$ , we anticipate that the sulfonyl groups of some [CTFSI] are weakly interacting with  $Li^+$  in addition to the coordinated cyano group. At  $x_{Li} = 0.5$  and 0.7, there is only a single peak that represents aggregates due to the full occupation of C=N sites on the anion (Figure 2c). This results in the broadening of N(≡C) symmetric stretch at 2220 cm<sup>-1</sup> which becomes indistinguishable from the aggregate peak at 2205 cm<sup>-1</sup>.

We see good correlation between experimental and simulated CN results for Li-N( $\equiv$ C) (**Figure 3**). However, the magnitude of the simulated CN for Li-O( $\equiv$ S) is overestimated. This is likely the result of setting the entire sulfonyl group as the COM for the RDF calculation, rather than the individual oxygens which results in a larger first solvation shell. Overestimation of sulfonyl coordination in mixed solvation environments is seen in previous MD studies. <sup>16</sup> As a result, it is

possible that  $Li^+$  that are not coordinated with the sulfonyl oxygens might be included in the CN if they are within the cut-off  $R_c$ .

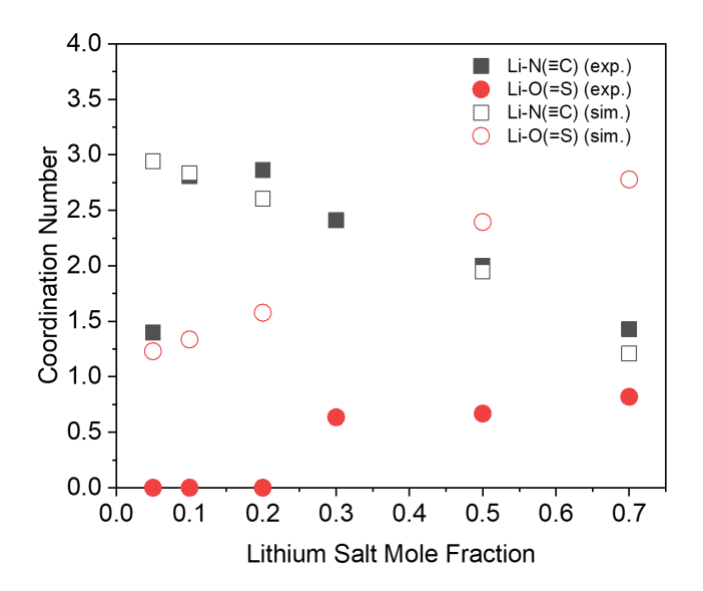


**Figure 3.** Dependence of CN for [PYR14][CTFSI] as a function of Li-salt mole fraction ( $x_{Li}$ ). Filled symbols represent experimentally calculated values and the hollow symbols represent the simulated results. Simulated CNs were found from the RDFs using an  $R_c$  of 325 pm for Li-N( $\equiv$ C) and 452 pm for Li-O( $\equiv$ S).

The computed RDFs and CNs are shown in **Figure 4** for CTFSI at  $x_{Li}$  = 0.05, 0.2, 0.5, and 0.7. For comparison, those for [TFSI], [DCA], and the [TFSI]:[DCA] mixture are shown in **Scheme S1**. The RDF in **Figure 4a** confirms little to no Li-O(=S) coordination at  $x_{Li}$  =0.05 relative to Li-N( $\equiv$ C) coordination. Increasing the concentration of Li<sup>+</sup> from  $x_{Li}$  =0.05 to  $x_{Li}$  =0.2 (**Figure 4b**), we see a slight decrease in the CN of Li-N( $\equiv$ C) and a slight increase in the CN of Li-O(=S), indicating that, with an increase in the amount of Li in the liquid, the Li cations prefer to coordinate via O(=S). This trend continues up until  $x_{Li}$ =0.7 (**Figure 4d**), where the Li-N( $\equiv$ C) CN has decreased by about 50% in comparison to  $x_{Li}$ =0.05, and Li-O(=S) accounts for most of the coordination. The

SDFs in **Figure 5** show how Li<sup>+</sup> or [PYR14] cations distribute around different anions. As  $x_{Li}$  increases, the [PYR14] cation is pushed out of the first solvation shell and replaced by Li<sup>+</sup>, up until  $x_{Li}$ =0.5, where [PYR14] is no longer visible. This is the case for the other anions ([TFSI] and [DCA]) studied (**Scheme S1**). From the green shell that first forms around the N( $\equiv$ C) at  $x_{Li}$ =0.05, it is again seen that N( $\equiv$ C) is the strongest associating site for Li<sup>+</sup>. While the SDF shows coordination sites on the O( $\equiv$ S) appearing at  $x_{Li}$ =0.2, the green Li<sup>+</sup> regions are much smaller on these sites than the green band surrounding the N( $\equiv$ C), indicating that coordination via the N( $\equiv$ C) is still dominating. Whereas, in moving to  $x_{Li}$ =0.5, the green bands surrounding the O( $\equiv$ S) are significantly larger, indicating larger contributions to coordination via the sulfonyl.

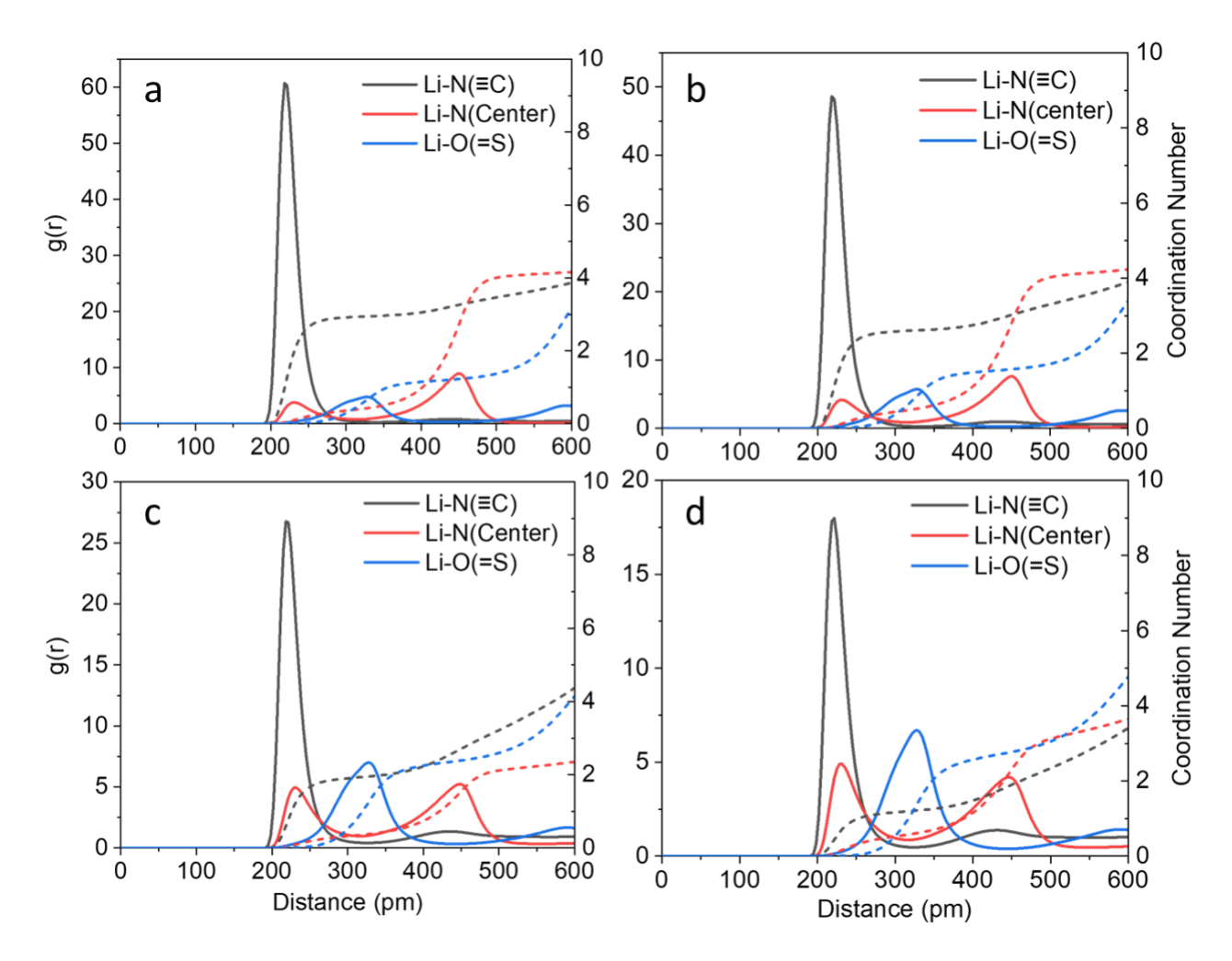


**Figure 4.** RDF (solid lines) and CNs (dotted lines) of Li<sup>+</sup>-[CTFSI] solvates for x<sub>Li</sub>=0.05 (**a**), 0.2 (**b**), 0.5 (**c**), and 0.7 (**d**).

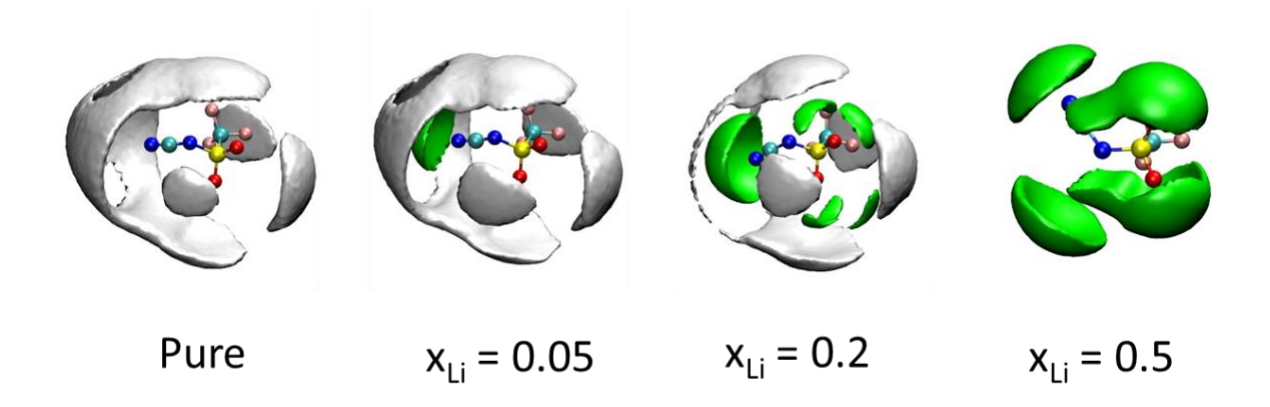


**Figure 5.** SDF images of [CTFSI] at varying Li-salt mole fractions at 328 K. Color code for atoms: red (O), yellow (S), blue (N), cyan (C), and rose (F). Green bands represent occupation of Li<sup>+</sup> and white bands represent occupation by [PYR14]. Simulations with  $x_{Li}$ =0.7 was only performed at 363 K and the SDF is similar to that of  $x_{Li}$ =0.5 shown here.

This structural behavior is further justified by the probabilities shown in **Figure 6**. The probability of Li<sup>+</sup> coordinating with the sulfonyl group are found to be less than 25% for  $x_{Li} \le 0.2$ , matching our Raman findings. A high probability of two Li<sup>+</sup> ions coordinating with the sulfonyl group at  $x_{Li} = 0.7$  (54%) suggests that all available cyano associating sites could be occupied, resulting in the monodentate coordination of 2 Li<sup>+</sup> via the sulfonyl group. This result further confirms the formation of ion-clusters in [CTFSI]. Cluster formation is much more likely at higher salt concentrations, where a probability of at least one Li<sup>+</sup> coordinating with via N( $\equiv$ C) and O( $\equiv$ S) are 96% and 94% at  $x_{Li} = 0.7$  and 88% and 76% at  $x_{Li} = 0.5$ , respectively. While the probabilities of coordination decrease as the Li-salt content decreases, the probability of at least one Li<sup>+</sup> coordinating with a sulfonyl group at  $x_{Li} = 0.2$  is 27% although we do not experimentally see any shift in the O( $\equiv$ S) symmetric stretch peak at 1120 cm<sup>-1</sup>. This confirms the likelihood of aggregate

formation and further justifies our peak deconvolution for the  $N(\equiv C)$  symmetric stretch into three peaks where the third peak is for the additional sulfonyl coordination on the same anion.

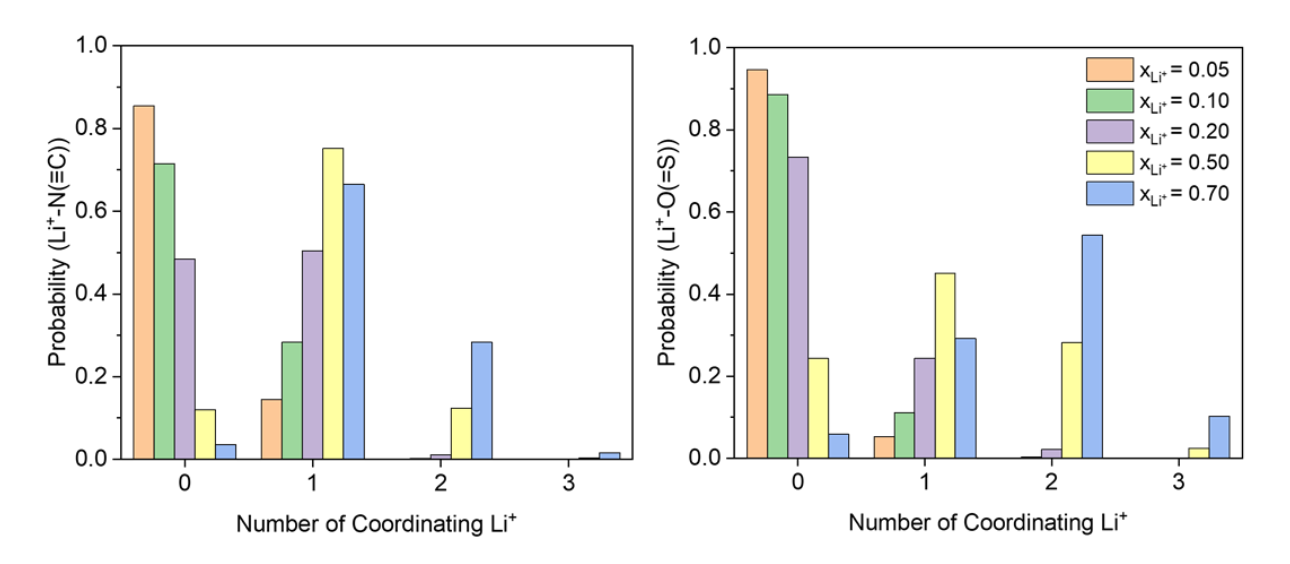


**Figure 6.** Probability of Li<sup>+</sup> coordinating with the cyano (Li<sup>+</sup>-N( $\equiv$ C)) and sulfonyl (Li<sup>+</sup>-O( $\equiv$ S)) sites of [CTFSI]. Probabilities are shown as a function of number of Li<sup>+</sup> (0 to 3).

The consistent trend that emerges from both the experimental and simulated coordination analysis is that Li-N( $\equiv$ C) coordination decreases as more Li<sup>+</sup> are introduced to the system, while the Li-O( $\equiv$ S) coordination increases with  $x_{Li} \geq 0.3$ . The emerging structure of the Li-solvate at  $0.3 < x_{Li} \leq 0.7$  is the coordination of two [CTSFI] anions, on average, with Li<sup>+</sup> in the first solvation shell. This is consistent with our previously computed energetically favored solvate structure of Li<sup>+</sup> with [CTFSI] using density functional theory.<sup>54</sup>

# Ion-pair lifetimes for Li<sup>+</sup>-[CTFSI] and the mixture of Li<sup>+</sup>-([DCA]:[TFSI])

The computed ion-pair lifetimes are shown in **Figure 7**. For [CTFSI], we separated the interactions of the O(=S) and the  $N(\equiv C)$ . Overall, the ion-pair lifetimes of the O(=S) of [CTFSI] are lower than

[DCA] in the [DCA]:[TFSI] mixture. In moving from  $x_{Li}$  of 0.05 to 0.2, the ion-pair lifetimes diverge even more, with [CTFSI] having roughly half of the lifetime when compared with [DCA]. This trend is again seen in the O(=S) coordination by [CTFSI] and [TFSI] in the [DCA]:[TFSI] mixture, where the ion-pair lifetimes of [CTFSI] are lower.

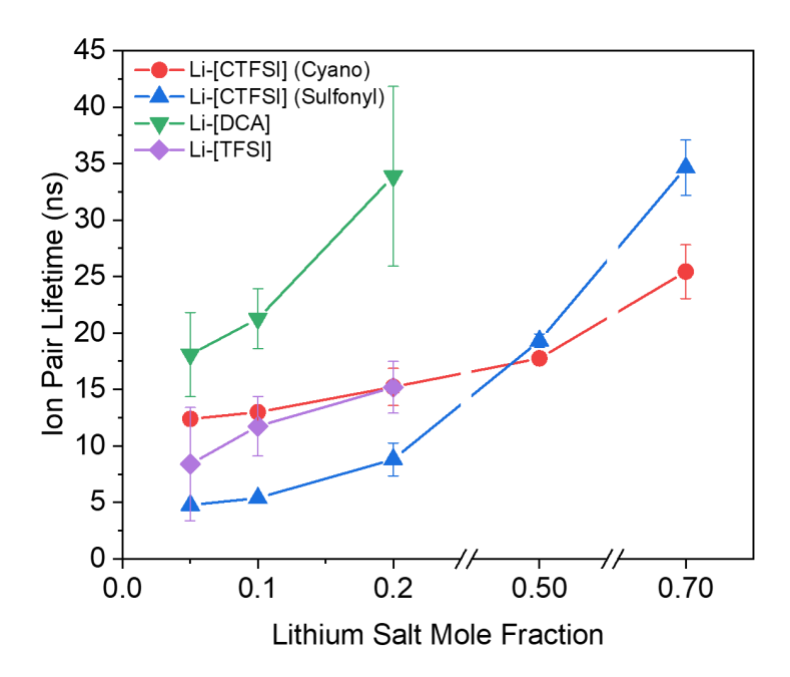


**Figure 7.** Ion-pair lifetimes for [PYR14][CTFSI] and [PYR14][TFSI]:[PYR14][DCA] as a function of Li-salt mole fraction  $(x_{Li})$ .

Some general observations can be noted from comparing the trends in the ion-pair lifetimes and the measured viscosities in the light of the Li<sup>+</sup> solvation structure examined. The stronger Li-N( $\equiv$ C) interaction leads to more rigid Li-solvates and the larger computed ion-pair lifetimes for Li-N( $\equiv$ C) confirm this. However, the bulk viscosity of the [DCA]:[TFSI] mixture electrolyte was smaller than the [CTFSI] system. This contrasts with the computed ion-pair lifetimes, which are expected to decrease with the smaller bulk viscosity. The best explanation for this observation is the smaller anion size of [DCA] that would result in smaller Li-solvates in which case the probability of

finding an appropriately sized void in the liquid to move to is higher. On the other hand, in the presence of [CTFSI], there seems to be more anion exchange especially compared to Li-[DCA] (comparing the red and green symbols in **Figure 7**). The weakest ionic association seems to be to the Li-O(=S) in [CTFSI] electrolyte (blue symbols in **Figure 7**) which is consistent with the lower coordination seen in Raman (red symbols in **Figure 3**). However, at  $x_{Li} \ge 0.5$  we see a shift in the trend, where the Li-O(=S) lifetime in [CTFSI] surpasses that of the Li-N( $\equiv$ C). At  $x_{Li} = 0.7$ , the ion pair lifetime of the Li-N( $\equiv$ C) for [CTFSI] is still lower than that for Li<sup>+</sup>-[DCA] at  $x_{Li} = 0.2$ . This result further indicates the relaxation of the first solvation structure in [CTFSI] at high salt concentrations.

#### **Diffusion Coefficients**

The simulated and experimental self-diffusivities are shown in **Figure 8** at 363K. The initial addition of Li-salt to the IL (i.e.,  $x_{Li}$  from 0 to 0.05) greatly decreases the mobility of the [PYR14] cation and the [CTFSI] anion. While the decrease in diffusivities with increased Li-salt concentration is consistently captured in both the experiments and simulations, the simulated values are significantly underestimated; interestingly this is the opposite of the trend in bulk viscosities of the simulated and experimentally measured [PYR14][CTFSI]. However, both the experimental and computational results agree that the diffusivity of Li<sup>+</sup> exceeds that of [CTFSI] at  $x_{Li} = 0.5$  and 0.7. We anticipate that the deviation between experimental and computed diffusivities, especially at higher concentrations ( $x_{Li} = 0.5$  and 0.7), is caused by a change in diffusion mechanism that is not captured by MD. At these higher concentrations, the diffusivity of Li<sup>+</sup> becomes larger than [CTFSI], suggesting a shift from vehicular to structural or 'hopping' diffusion, as the anion is now lagging behind Li<sup>+</sup>, which would lead to the exchange of anions

within the first solvation shell. This change in ion transport method is also apparent in the Arrhenius plot shown in **Figure S8**. The activation energies increase as  $x_{Li}$  increases up to a concentration of 0.3 (0.376 eV), however, in moving to  $x_{Li} = 0.5$ , the activation energy decreases by half (0.186 eV). This is in contrast to the expected increase in activation energy for the more viscous  $x_{Li} = 0.5$  electrolyte compared to  $x_{Li} = 0.3$  since the solvation shell around Li<sup>+</sup> would experience greater hindrance in transport in more viscous media. This change in activation energy indicates that there must be change in the conduction of ions in solution.

The measured and simulated diffusivities as a function of temperature are given **Table S5 and Figure S9**, and the computational diffusivities for [DCA], [TFSI], and [DCA]:[TFSI] mixture are plotted in **Scheme 1**. As expected, the diffusivities increased with temperature. From the VFT fits, the estimated viscosity for the IL electrolyte at  $x_{Li} = 0.2$  reduces from 378 cP at 298 K to about 37 cP at 363 K. Although, the viscosities are not available for  $x_{Li} = 0.5$  or 0.7 due to gel formation, we expect viscosity reduction with increased temperature, similarly to the characterized compositions. The diffusivities of [PYR14][DCA] and [PYR14][TFSI] were also computed in comparison to the [DCA]:[TFSI] mixture system. Overall, the diffusivities followed the opposite trend in the ion size as  $D_{[TFSI]} < D_{[PYR14]} < D_{[DCA]}$  whereas  $D_{[CTFSI]}$  was the weighted average of  $D_{[TFSI]}$  and  $D_{[DCA]}$ ; consistent with the ideal mixing.

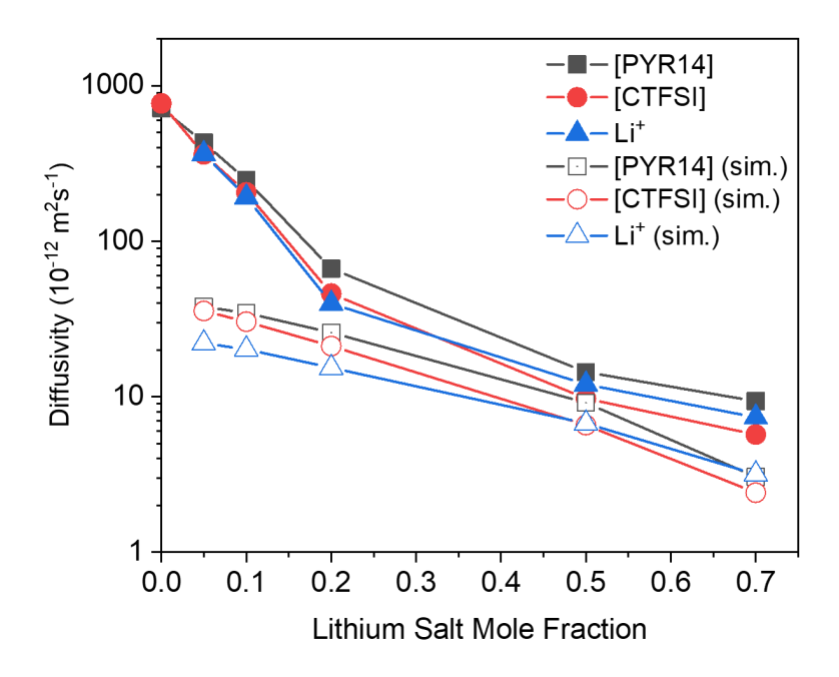


**Figure 8.** Simulated (hollow symbols) and experimental (filled symbols) diffusivities for [PYR14][CTFSI] (**a**) and [PYR14][DCA]:[PYR14][TFSI] (**b**) systems as a function of Li-salt mole fraction (x<sub>Li</sub>). Both simulated and experimental diffusivities were obtained at 363K.

The calculated Li<sup>+</sup> transference numbers from the experimental measured diffusivities,  $t_{NMR}^+$  (at 298K, 328K, and 363K) and simulated diffusivities,  $t_{sim}^+$  (328K and 363K) for both the [CTFSI] and the [TFSI]:[DCA] systems are in **Table 4**. The simulated and experimental  $t^+$  at both 328K and 363K show good agreement. Overall, the  $t_{NMR}^+$  for  $x_{Li} \ge 0.5$  were found to be higher due to the higher mobility of Li<sup>+</sup> compared to [CTFSI]. For  $x_{Li} = 0.05$ ,  $t_{sim}^+$  at 328K is estimated to be larger in [CTFSI] system compared to the [DCA]:[TFSI] mixture. This is in line with the shorter ion-pair lifetimes calculated for Li-O(=S) and Li-N(=C) in [CTFSI]. While the concentrations examined in these studies are low for [TFSI]:[DCA], the higher  $t_{sim}^+$  and shorter ion-pair lifetime may be indicative of structural fluctuations induced at the micro-scale by the asymmetric anion [CTFSI] even though the bulk viscosities are higher with [CTFSI] at the macro-scale.

**Table 2.** Experimental  $(t_{NMR}^+)$  at 299K, 328K, 363K) and simulated  $(t_{sim}^+)$  at 328K and 363K) Li<sup>+</sup> transference numbers for [PYR14][CTFSI] and [PYR14][DCA]:[PYR14][TFSI] electrolytes. Experimental transference numbers for the [DCA]:[TFSI] mixture could not be calculated, as  $C^{13}$  NMR was not able to resolve the  $C \equiv N$  group from the  $CF_3$ .

IL Anion	$\mathbf{x}_{\mathrm{Li}}$	t <sub>NMR</sub> (299K)	t <sub>NMR</sub> (328K)	t <sub>NMR</sub> (363K)	t <sub>sim</sub> (328K)	t <sub>sim</sub> (363K)
[CTFSI]	0.05	0.168	0.177	0.315	0.205	0.231
	0.1	0.173	0.178	0.298	0.224	0.237
	0.2	0.174	0.196	0.261	0.226	0.246
	0.5	0.160	0.142	0.332	_	0.300
	0.7	0.188	0.214	0.328	_	0.367
[DCA]:[TFSI]	0.05	_	_	_	0.142	_

# **Electrochemical Stability**

In order to provide an initial assessment and perspective on the utility of the [PYR14][CTFSI] as an electrolyte for LIBs, the electrochemical stability window was measured (**Figure 9**). This was further compared to those electrolytes with the analogous symmetric anions and anion mixtures. The [PYR14][CTFSI] based electrolytes possess a larger anodic stability window compared to [PYR14][DCA]:[PYR14][TFSI] based electrolytes. The [PYR14][DCA]:[PYR14][TFSI] system starts to decompose around 1.3 V (*vs.* Pt), where a sharp increase in current is seen and followed by a decrease at higher potentials. The suppressed current at higher potentials is likely due to the passivation of the electrode surface by the decomposed [DCA]. This is suggesting that substitution of a -CN group with a -SO<sub>2</sub>-CF<sub>3</sub> can improve the anodic stability of the [PYR14][CTFSI] based

electrolytes<sup>26</sup>. It can be seen that incorporation of Li-salt increased the cathodic stability of both ILs electrolytes. As for [PYR14][CTFSI] based electrolytes, both the cathodic and anodic stabilities enhanced upon salt addition, leading to an improved stability window of 4.65 V at  $x_{Li}$  = 0.3 compared to 4.25 V (neat IL).

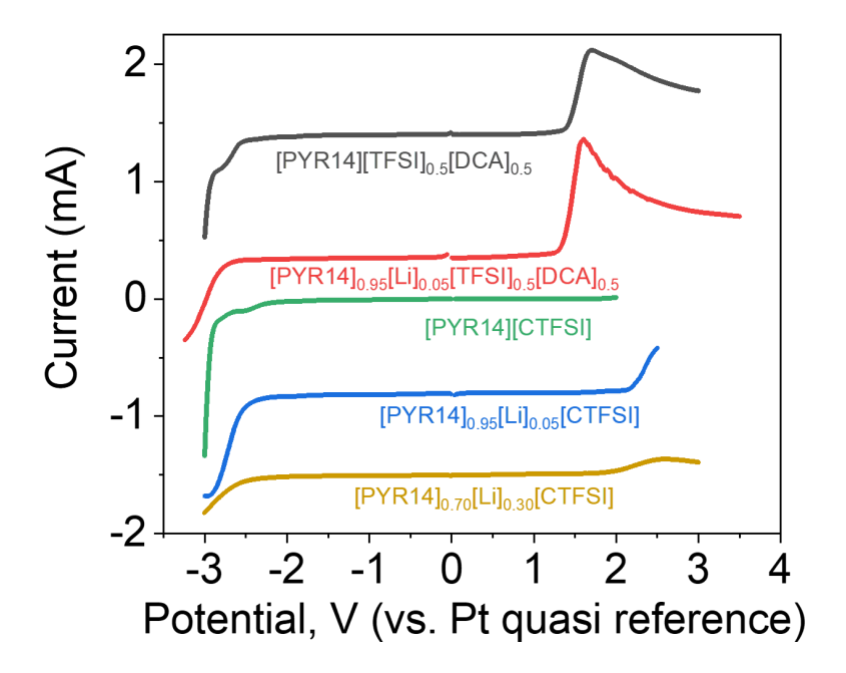


**Figure 9.** Electrochemical stability windows of the ILs and IL electrolytes, with currents offset for easier visualization. LSVs were performed at a scan rate of 20 mV s<sup>-1</sup> with a GC working electrode and Pt counter and quasi-reference electrodes.

# Rate Capability and Cycling of Li-LFP

**Figure 10a** shows the charge-discharge curves of Li-LFP coin cells prepared with [PYR14][CTFSI] electrolytes with  $x_{Li} = 0.3$ , 0.5, and 0.7. The capacities of all three cells at 0.1C at 298 K are low due to the high viscosity, poor electrode wettability, and slow diffusion of Li<sup>+</sup> which resulted in large over potentials of the electrolytes. When temperature was increased to 363

K, the cells capacities were measured to be in the range of 140-150 mAh/g, which is close to the theoretical value of 170 mAh/g for LFP. Cells with  $x_{Li} = 0.5$  and 0.7 demonstrated similar overpotential upon lithiation (3.52 V) as well as delithiation (3.36 V) (**Figure 10a**). The cell with  $x_{Li}$ = 0.3 demonstrated the highest capacity retention as the cycling C-rate increased (Figure 10b), corresponding to its higher Li<sup>+</sup> diffusivity (**Figure 8**). On the other hand, the cell with  $x_{Li} = 0.7$ was found to be the most thermodynamically stable (on cathodic and anodic side) at 363 K and demonstrated the highest capacity retention upon returning from 1 C to 0.2 C. This result is significant to the field of Li and Li-ion batteries, as the current state-of-the-art carbonate electrolytes are not be stable at such high temperatures, and would result in rapid cell failure due to the volatilization of the electrolyte. In contrast, the cell with  $x_{Li} = 0.5$  undergoes severe side reactions at 1 C, where thick solid-electrolyte interphase layer may form on the electrode interfaces as suggested by the low Coulombic efficiency of 60 to 90% (Figure 10b). This is also confirmed by the drastic increase of the impedance (both SEI impedance and charge transfer impedance) by comparing the red dashed line with the red solid line in **Figure 10c**. The impedance increase for  $x_{Li} = 0.3$  and 0.7 electrolyte is not as significant. CV results in Figure 10d also shows the reversibility of the  $Fe^{2+}/Fe^{3+}$  redox in the LFP electrode is sluggish with the  $x_{Li}=0.5$  electrolyte which can help explain the low Coulombic efficiency.

The Li<sup>+</sup> diffusivity within LFP electrode was measured by the GITT and found to be in the order of  $10^{-15}$  m<sup>2</sup>s<sup>-1</sup> at the beginning of the charging step then decreased exponentially as Li<sup>+</sup> gradually depleted at the interphase (**Figure 10e**). The diffusivities of Li<sup>+</sup> in the x<sub>Li</sub>=0.3 and 0.5 cell are similar if not higher than that of x<sub>Li</sub> = 0.7 cell across the whole de-lithiation process. This is in contrast to the lower overall diffusivities seen in x<sub>Li</sub> = 0.7, further indicating beneficial interfacial

interactions in the more concentrated electrolyte. **Figure 10f** shows the cyclability at 0.1 C of the same cells. The capacity retention of  $x_{Li} = 0.7$  cell was observed to be the highest. Therefore, we conclude the better cyclability of  $x_{Li} = 0.7$  cell to be ascribed to its stable electrolyte-electrode interface and increased diffusivity of  $Li^+$  in comparison to [CTFSI], resulting in enhanced  $Li^+$  transport in the electrolyte via structural diffusion or 'hopping'.

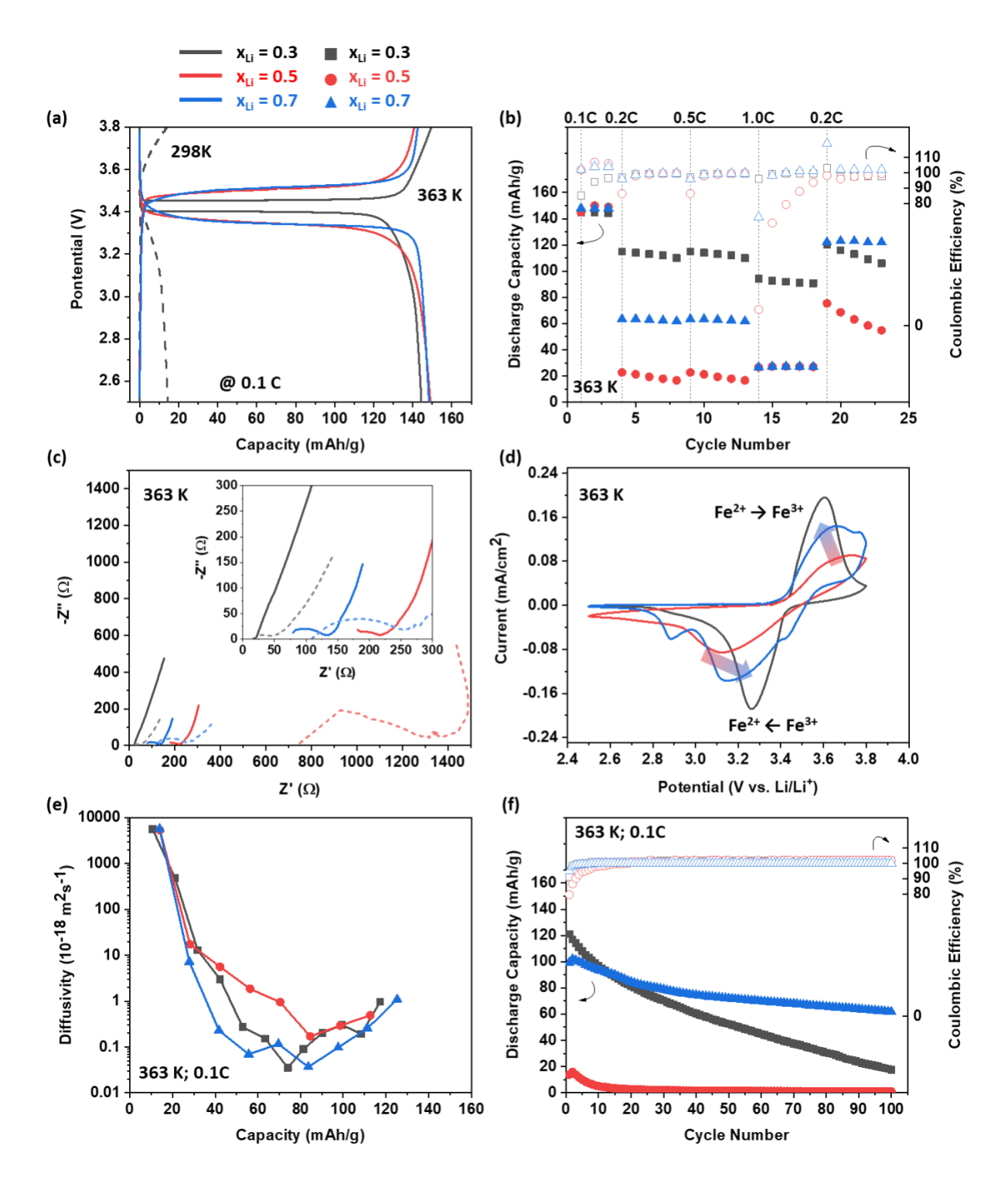


**Figure 10.** (a) Charge-discharge curves at 298 K (dashed line) and at 363 K (solid line), corresponding to the 3<sup>rd</sup> cycle at 0.1 C. (b) Rate capability test at 0.1, 0.2, 0.5, 1 C and then again 0.2 C at 363 K. (c) EIS of the LIBs before (solid line) and after (dashed line) the rate capability

test. The inset shows the magnified EIS spectra at low impedance region. (d) CV of the same Li-LFP cells after the rate capability test at 363 K, at a scanning rate of 0.05 mV/s. (e) Diffusivity of Li<sup>+</sup> in LFP electrode in the charging process, calculated via the GITT method. An example of a GITT potential profile is given in **Figure S10**. (f) Cyclability at 363 K and 0.1 C rate following the GITT sequences.

#### **Conclusions**

In this work, we examined the physical properties, solvation dynamics, and electrochemical stability of [PYR14][CTSFI] and its mixture with [Li][CTFSI] in comparison to the binary mixture of [PYR14][DCA]:[PYR14][TFSI] and its corresponding electrolyte with [Li][TFSI]. The measured density, viscosity, and conductivity of [PYR14][CTSFI] is found to correspond to the weighted average of that of the [DCA]:[TFSI] system. However, the solubility of the Li-salt is found to be significantly higher in the electrolyte with the asymmetric anion. From the CN analysis, both the [CTFSI] and [DCA]:[TFSI] systems preferentially coordinate with Li<sup>+</sup> via the cyano group, up until  $x_{Li} = 0.3$ , where sulfonyl coordination becomes noticeable. The competition between the cyano and sulfonyl groups on the same anion for Li<sup>+</sup> coordination results in weaker solvation by [CTFSI], which is confirmed by Li<sup>+</sup>-[CTFSI] having shorter ion-pair lifetimes compared to symmetric anions. The transference numbers calculated from NMR and MD showed high overall transference for [CTFSI]-based systems, indicating that the asymmetry of [CTFSI] allows for high relative mobility of Li<sup>+</sup>, especially at high concentrations. These results suggest the possibly improved Li<sup>+</sup> concentration and transport in IL electrolytes with asymmetric anions. Moreover, evaluation of the electrochemical window shows improved stability by asymmetric anion and higher Li<sup>+</sup> salt concentration as opposed to the electrolytes with the symmetric anion.

Indeed, the Li-LFP cells with  $x_{Li} = 0.7$  was observed to be the most thermodynamic stable one, as confirmed by the long term battery-cycling tests.

# **Supporting Information**

Table of electrolyte compositions, tables of experimental and computed densities, viscosities and conductivities, VFT fit parameters, images of the samples, Raman fits, computed RDFs, Computed SDFs with discussion and CNs, Arrhenius plot of conductivity, simulated diffusivities, GITT potential curves, and an example input file for the MD simulations.

#### **Author contributions**

D.P. performed the physical property measurements, Raman analysis and facilitated the synergy between the experiments and computations. X.W. performed MD simulations and the computational analysis. M.G. performed the NMR measurements. R.G. performed the electrochemical measurements. Y.Y. Lee performed the LIB tests. S.G. led the discussions on diffusivities. E.J.M. oversaw the computational methods and analysis. B.G. developed the plan of study and led the general discussions. All authors contributed to the writing of the manuscript.

# Acknowledgements

The property measurements, Raman analysis and LIB tests were supported by NSF CBET Award No. 1903259. D.P. and B.G. would like to thank the Center for Applied Raman Spectroscopy (CWRU). X.W. was supported by Breakthrough Electrolytes for Energy Storage (BEES), an Energy Frontier Research Center funded by the U.S. Department of Energy, Office of Science, Basic Energy Science under award number DE-SC0019409. X.W. and E.J.M. acknowledge Notre

Dame's Center for Research Computing. Y.Y Lee would like to thank Lin Li for the assistance with the Python script for GITT data analysis.

#### References

- 1. Borgel, V.; Markevich, E.; Aurbach, D.; Semrau, G.; Schmidt, M., On the application of ionic liquids for rechargeable Li batteries: High voltage systems. *J. Power Sources* **2009**, *189* (1), 331-336.
- 2. Armand, M.; Endres, F.; MacFarlane, D. R.; Ohno, H.; Scrosati, B., Ionic-liquid materials for the electrochemical challenges of the future. *Nature Materials* **2009**, *8* (8), 621-629.
- 3. Eftekhari, A.; Liu, Y.; Chen, P., Different roles of ionic liquids in lithium batteries. *J. Power Sources* **2016**, *334*, 221-239.
- 4. Navarra, M. A., Ionic liquids as safe electrolyte components for Li-metal and Li-ion batteries. *Mrs Bulletin* **2013**, *38* (7), 548-553.
- 5. Bae, S.-Y.; Shim, E.-G.; Kim, D.-W., Effect of ionic liquid as a flame-retarding additive on the cycling performance and thermal stability of lithium-ion batteries. *J. Power Sources* **2013**, *244*, 266-271.
- 6. Galinski, M.; Lewandowski, A.; Stepniak, I., Ionic liquids as electrolytes. *Electrochim. Acta* **2006,** *51* (26), 5567-5580.
- 7. Nasrabadi, A. T.; Ganesan, V., Structure and Transport Properties of Lithium-Doped Aprotic and Protic Ionic Liquid Electrolytes: Insights from Molecular Dynamics Simulations. *Journal of Physical Chemistry B* **2019**, *123* (26), 5588-5600.
- 8. Gehrke, S.; von Domaros, M.; Clark, R.; Holloczki, O.; Brehm, M.; Welton, T.; Luzar, A.; Kirchner, B., Structure and lifetimes in ionic liquids and their mixtures. *Faraday Discussions* **2018**, *206*, 219-245.
- 9. Haskins, J. B.; Bennett, W. R.; Wu, J. J.; Hernández, D. M.; Borodin, O.; Monk, J. D.; Bauschlicher, C. W.; Lawson, J. W., Computational and Experimental Investigation of Li-Doped Ionic Liquid Electrolytes: [pyr14][TFSI], [pyr13][FSI], and [EMIM][BF4]. *The Journal of Physical Chemistry B* **2014**, *118* (38), 11295-11309.
- 10. Gao, X.; Wu, F.; Mariani, A.; Passerini, S., Concentrated Ionic-Liquid-Based Electrolytes for High-Voltage Lithium Batteries with Improved Performance at Room Temperature. *ChemSusChem* **2019**, *12* (18), 4185-4193.
- 11. Heist, A.; Lee, S.-H., Improved Stability and Rate Capability of Ionic Liquid Electrolyte with High Concentration of LiFSI. *Journal of The Electrochemical Society* **2019**, *166* (10), A1860-A1866.
- 12. Forsyth, M.; Yoon, H.; Chen, F.; Zhu, H.; MacFarlane, D. R.; Armand, M.; Howlett, P. C., Novel Na+ Ion Diffusion Mechanism in Mixed Organic–Inorganic Ionic Liquid Electrolyte Leading to High Na+ Transference Number and Stable, High Rate Electrochemical Cycling of Sodium Cells. *The Journal of Physical Chemistry C* **2016**, *120* (8), 4276-4286.
- 13. Kerner, M.; Plylahan, N.; Scheers, J.; Johansson, P., Ionic liquid based lithium battery electrolytes: fundamental benefits of utilising both TFSI and FSI anions? *Physical Chemistry Chemical Physics* **2015**, *17* (29), 19569-19581.
- 14. Chen, F. F.; Forsyth, M., Computational Investigation of Mixed Anion Effect on Lithium Coordination and Transport in Salt Concentrated Ionic Liquid Electrolytes. *Journal of Physical Chemistry Letters* **2019**, *10* (23), 7414-7420.

- 15. Huang, Q.; Lee, Y.-Y.; Gurkan, B., Pyrrolidinium Ionic Liquid Electrolyte with Bis(trifluoromethylsulfonyl)imide and Bis(fluorosulfonyl)imide Anions: Lithium Solvation and Mobility, and Performance in Lithium Metal–Lithium Iron Phosphate Batteries. *Industrial & Engineering Chemistry Research* **2019**.
- 16. Huang, Q.; Lourenço, T. C.; Costa, L. T.; Zhang, Y.; Maginn, E. J.; Gurkan, B., Solvation Structure and Dynamics of Li+ in Ternary Ionic Liquid–Lithium Salt Electrolytes. *The Journal of Physical Chemistry B* **2019**, *123* (2), 516-527.
- 17. Chaudoy, V.; Jacquemin, J.; Tran-Van, F.; Deschamps, M.; Ghamouss, F., Effect of mixed anions on the transport properties and performance of an ionic liquid-based electrolyte for lithium-ion batteries. *Pure and Applied Chemistry* **2019**, *91* (8), 1361-1381.
- 18. Bayley, P. M.; Best, A. S.; MacFarlane, D. R.; Forsyth, M., Transport Properties and Phase Behaviour in Binary and Ternary Ionic Liquid Electrolyte Systems of Interest in Lithium Batteries. *ChemPhysChem* **2011**, *12* (4), 823-827.
- 19. Lesch, V.; Li, Z.; Bedrov, D.; Borodin, O.; Heuer, A., The influence of cations on lithium ion coordination and transport in ionic liquid electrolytes: a MD simulation study. *Physical Chemistry Chemical Physics* **2016**, *18* (1), 382-392.
- 20. Brinkkötter, M.; Giffin, G. A.; Moretti, A.; Jeong, S.; Passerini, S.; Schönhoff, M., Relevance of ion clusters for Li transport at elevated salt concentrations in [Pyr12O1][FTFSI] ionic liquid-based electrolytes. **2018**.
- 21. Giffin, G. A.; Moretti, A.; Jeong, S.; Pilar, K.; Brinkkötter, M.; Greenbaum, S. G.; Schönhoff, M.; Passerini, S., Connection between Lithium Coordination and Lithium Diffusion in [Pyr12O1][FTFSI] Ionic Liquid Electrolytes. *ChemSusChem* **2018**, *11* (12), 1981-1989.
- 22. Nurnberg, P.; Lozinskaya, E. I.; Shaplov, A. S.; Schonhoff, M., Li Coordination of a Novel Asymmetric Anion in Ionic Liquid-in-Li Salt Electrolytes. *Journal of Physical Chemistry B* **2020**, *124* (5), 861-870.
- 23. Giffin, G. A.; Moretti, A.; Jeong, S.; Passerini, S., Decoupling effective Li+ ion conductivity from electrolyte viscosity for improved room-temperature cell performance. *J. Power Sources* **2017**, *342*, 335-341.
- 24. Yoon, H.; Best, A. S.; Forsyth, M.; MacFarlane, D. R.; Howlett, P. C., Physical properties of high Li-ion content N-propyl-N-methylpyrrolidinium bis(fluorosulfonyl)imide based ionic liquid electrolytes. *Physical Chemistry Chemical Physics* **2015**, *17* (6), 4656-4663.
- 25. Henderson, W. A.; Passerini, S., Phase Behavior of Ionic Liquid–LiX Mixtures: Pyrrolidinium Cations and TFSI- Anions. *Chemistry of Materials* **2004**, *16* (15), 2881-2885.
- 26. Hoffknecht, J. P.; Drews, M.; He, X.; Paillard, E., Investigation of the N-butyl-N-methyl pyrrolidinium trifluoromethanesulfonyl-N-cyanoamide (PYR(14)TFSAM) ionic liquid as electrolyte for Li-ion battery. *Electrochim. Acta* **2017**, *250*, 25-34.
- 27. Bruce, P. G.; Evans, J.; Vincent, C. A., CONDUCTIVITY AND TRANSFERENCE NUMBER MEASUREMENTS ON POLYMER ELECTROLYTES. *Solid State Ion.* **1988**, *28*, 918-922.
- 28. Stejskal, E. O.; Tanner, J. E., Spin Diffusion Measurements: Spin Echoes in the Presence of a Time-Dependent Field Gradient. *The Journal of Chemical Physics* **1965**, *42* (1), 288-292.
- 29. Sälzer, F.; Pateras Pescara, L.; Franke, F.; Müller, C.; Winkler, J.; Schwalm, M.; Roling, B., Assessing the Ion Transport Properties of Highly Concentrated Non-Flammable

- Electrolytes in a Commercial Li-Ion Battery Cell. *Batteries & Supercaps* **2020**, *3* (1), 117-125.
- 30. Chen, L. Y.; Fu, J. F.; Lu, Q.; Shi, L. Y.; Li, M. M.; Dong, L. N.; Xu, Y. F.; Jia, R. R., Cross-linked polymeric ionic liquids ion gel electrolytes by in situ radical polymerization. *Chem. Eng. J.* **2019**, *378*, 8.
- 31. Pesko, D. M.; Timachova, K.; Bhattacharya, R.; Smith, M. C.; Villaluenga, I.; Newman, J.; Balsara, N. P., Negative Transference Numbers in Poly(ethylene oxide)-Based Electrolytes. *Journal of The Electrochemical Society* **2017**, *164* (11), E3569-E3575.
- 32. Balsara, N. P.; Newman, J., Relationship between Steady-State Current in Symmetric Cells and Transference Number of Electrolytes Comprising Univalent and Multivalent Ions. *Journal of The Electrochemical Society* **2015**, *162* (14), A2720-A2722.
- 33. Duluard, S.; Grondin, J.; Bruneel, J.-L.; Pianet, I.; Grélard, A.; Campet, G.; Delville, M.-H.; Lassègues, J.-C., Lithium solvation and diffusion in the 1-butyl-3-methylimidazolium bis(trifluoromethanesulfonyl)imide ionic liquid. *J. Raman Spectrosc.* **2008**, *39* (5), 627-632.
- 34. Chauvin, C.; Alloin, F.; Judeinstein, P.; Foscallo, D.; Sanchez, J. Y., Electrochemical and NMR characterizations of mixed polymer electrolytes based on oligoether sulfate and imide salts. *Electrochimica Acta* **2006**, *52* (3), 1240-1246.
- 35. Vogel, H., Das Temperaturabhangigkeitsgesetz der Viskositat von Flussigkeiten. *Phys. Z.* **1921,** *22*, 645-646.
- 36. Fulcher, G. S., ANALYSIS OF RECENT MEASUREMENTS OF THE VISCOSITY OF GLASSES. *Journal of the American Ceramic Society* **1925**, *8* (6), 339-355.
- 37. Lassègues, J.-C.; Grondin, J.; Aupetit, C.; Johansson, P., Spectroscopic Identification of the Lithium Ion Transporting Species in LiTFSI-Doped Ionic Liquids. *The Journal of Physical Chemistry A* **2009**, *113* (1), 305-314.
- 38. Wang, J.; Wolf, R. M.; Caldwell, J. W.; Kollman, P. A.; Case, D. A., Development and testing of a general amber force field. *Journal of computational chemistry* **2004,** *25* (9), 1157-1174.
- 39. Frisch, M. J.; Trucks, G. W.; Schlegel, H. B.; Scuseria, G. E.; Robb, M. A.; Cheeseman, J. R.; Scalmani, G.; Barone, V.; Petersson, G. A.; Nakatsuji, H.; Li, X.; Caricato, M.; Marenich, A. V.; Bloino, J.; Janesko, B. G.; Gomperts, R.; Mennucci, B.; Hratchian, H. P.; Ortiz, J. V.; Izmaylov, A. F.; Sonnenberg, J. L.; Williams; Ding, F.; Lipparini, F.; Egidi, F.; Goings, J.; Peng, B.; Petrone, A.; Henderson, T.; Ranasinghe, D.; Zakrzewski, V. G.; Gao, J.; Rega, N.; Zheng, G.; Liang, W.; Hada, M.; Ehara, M.; Toyota, K.; Fukuda, R.; Hasegawa, J.; Ishida, M.; Nakajima, T.; Honda, Y.; Kitao, O.; Nakai, H.; Vreven, T.; Throssell, K.; Montgomery Jr., J. A.; Peralta, J. E.; Ogliaro, F.; Bearpark, M. J.; Heyd, J. J.; Brothers, E. N.; Kudin, K. N.; Staroverov, V. N.; Keith, T. A.; Kobayashi, R.; Normand, J.; Raghavachari, K.; Rendell, A. P.; Burant, J. C.; Iyengar, S. S.; Tomasi, J.; Cossi, M.; Millam, J. M.; Klene, M.; Adamo, C.; Cammi, R.; Ochterski, J. W.; Martin, R. L.; Morokuma, K.; Farkas, O.; Foresman, J. B.; Fox, D. J. *Gaussian 16 Rev. B.01*, Wallingford, CT, 2016.
- 40. Bayly, C. I.; Cieplak, P.; Cornell, W.; Kollman, P. A., A well-behaved electrostatic potential based method using charge restraints for deriving atomic charges: the RESP model. *The Journal of Physical Chemistry* **1993**, *97* (40), 10269-10280.

- 41. Wang, J.; Wang, W.; Kollman, P. A.; Case, D. A., Automatic atom type and bond type perception in molecular mechanical calculations. *Journal of molecular graphics and modelling* **2006**, *25* (2), 247-260.
- 42. Kirby, B. J.; Jungwirth, P., Charge Scaling Manifesto: A Way of Reconciling the Inherently Macroscopic and Microscopic Natures of Molecular Simulations. *The Journal of Physical Chemistry Letters* **2019**, *10* (23), 7531-7536.
- 43. Plimpton, S., Fast parallel algorithms for short-range molecular dynamics. *Journal of computational physics* **1995**, *117* (1), 1-19.
- 44. Brehm, M.; Thomas, M.; Gehrke, S.; Kirchner, B., TRAVIS—A free analyzer for trajectories from molecular simulation. *The Journal of chemical physics* **2020**, *152* (16), 164105.
- 45. Brehm, M.; Kirchner, B., TRAVIS-a free analyzer and visualizer for Monte Carlo and molecular dynamics trajectories. ACS Publications: 2011.
- 46. Hockney, R.; Eastwood, J., Computer Simulation Using Particles (Adam Hilger, New York). **1989**.
- 47. Martínez, L.; Andrade, R.; Birgin, E. G.; Martínez, J. M., PACKMOL: a package for building initial configurations for molecular dynamics simulations. *Journal of computational chemistry* **2009**, *30* (13), 2157-2164.
- 48. Zhang, Y.; Otani, A.; Maginn, E. J., Reliable viscosity calculation from equilibrium molecular dynamics simulations: A time decomposition method. *Journal of chemical theory and computation* **2015**, *11* (8), 3537-3546.
- 49. Noda, A.; Hayamizu, K.; Watanabe, M., Pulsed-Gradient Spin–Echo 1H and 19F NMR Ionic Diffusion Coefficient, Viscosity, and Ionic Conductivity of Non-Chloroaluminate Room-Temperature Ionic Liquids. *The Journal of Physical Chemistry B* **2001**, *105* (20), 4603-4610.
- 50. Kubisiak, P.; Eilmes, A., Estimates of Electrical Conductivity from Molecular Dynamics Simulations: How to Invest the Computational Effort. *The Journal of Physical Chemistry B* **2020**, *124* (43), 9680-9689.
- 51. Haskins, J. B.; Bennett, W. R.; Wu, J. J.; Hernández, D. M.; Borodin, O.; Monk, J. D.; Bauschlicher Jr, C. W.; Lawson, J. W., Computational and experimental investigation of Lidoped ionic liquid electrolytes:[pyr14][TFSI],[pyr13][FSI], and [EMIM][BF4]. *The Journal of Physical Chemistry B* **2014**, *118* (38), 11295-11309.
- 52. Mendez-Morales, T.; Carrete, J.; Bouzon-Capelo, S.; Perez-Rodriguez, M.; Cabeza, O.; Gallego, L. J.; Varela, L. M., MD simulations of the formation of stable clusters in mixtures of alkaline salts and imidazolium-based ionic liquids. *The Journal of Physical Chemistry B* **2013**, *117* (11), 3207-3220.
- 53. Lourenço, T. C.; Zhang, Y.; Costa, L. T.; Maginn, E. J., A molecular dynamics study of lithium-containing aprotic heterocyclic ionic liquid electrolytes. *The Journal of chemical physics* **2018**, *148* (19), 193834.
- 54. Penley, D.; Vicchio, S. P.; Getman, R. B.; Gurkan, B., Energetics of Li+ Coordination with Asymmetric Anions in Ionic Liquids by Density Functional Theory. *Frontiers in Energy Research* **2021**, *9* (570).

# **Table of Content Figure**

